Marine-Fouling Composition Estimation using Cost-effective Sensing

Mai, Christian; Sørensen, Fredrik Fogh; Liniger, Jesper; Pedersen, Simon

Published in:
Proceedings of the OCEANS 2024 - Halifax

DOI (link to publication from Publisher):
10.1109/OCEANS55160.2024.10754572

Publication date:
2024

Document Version
Accepted author manuscript, peer reviewed version

Marine-Fouling Composition Estimation using Cost-effective Sensing

Christian Mai*, Fredrik F. Sørensen*, Jesper Liniger*, Simon Pedersen*
*AAU Energy, Aalborg University, Esbjerg, Denmark, (Email: chrimai@energy.aau.dk)

***Abstract*—Determination of coverage and thickness of marine growth is a useful tool for determining structural loads and drags on marine structures and ships. In this work, we present an algorithmic program based on sonar and optical camera measurements, that estimates both the coverage and thickness of marine-fouling on off-shore structures. The marine-fouling composition is estimated using a Deep-Neural Network, trained using supervised methods, which can distinguish between hard/soft fouling species and the background water and structural components. The marine-fouling thickness is estimated using an HF Forward Looking Sonar, which is applied as a sensitive ultrasonic thickness gauge, when combined with a thickness measurement algorithm. Combined the measurements provide a localized estimate of the marine-fouling coverage and loadings across the structural surfaces, which can be used for automatic inspection evaluation and mission planning.**
Keywords: marine-fouling, deep-neural-network, visual sensing, acoustic sensing

I. Introduction

Marine growth causes offshore structures to suffer from increased mechanical loads, in the form of increased weight and wave-loads due to surface roughness [1]. Thus, estimating the coverage and thickness of marine fouling is a useful and relevant tool for determining structural loads and hydrodynamic drags on coastal and offshore marine structures, thereby contributing to the structural integrity management as it relates to marine-growth loading; automation of marine-growth inspection provides additional benefits in decreasing cost while increasing frequency and quality of growth estimation [2]. Methods to evaluate the marine-growth were explored for various load scenarios: In [3], the marine-growth load on mooring lines has been investigated using automation built on top of a manual visual ruler gauge tool, while relatedly, in [4], fractal dimensions were explored as a descriptive parameter to characterize marine-fouling load. For fixed offshore structures, the marine-growth causes additional loads mostly caused by increased hydrodynamic drag interactions through wave forces, this has been explored for several structural elements such as individual cylindrical structural elements [5], while complete jacket offshore structures were explored in [6] and [7].

In this work, we present an algorithmic approach based on sonar and RGB optical camera measurements, that estimates both the percentage surface coverage and thickness of marine-fouling on off-shore structures. The marine-fouling thickness is estimated using a commercial off-the-shelf High-frequency Forward Looking Sonar, which is applied as a sensitive ultrasonic thickness gauge when combined with a thickness measurement algorithm. The marine-fouling composition is estimated using a Deep-Neural Network, trained using synthetic data-based supervised methods, which can distinguish between hard/soft fouling species and the background water and structural components. Combined the measurements provide a highly detailed estimate of the marine-fouling coverage and loadings across the structural surfaces, which can be used for automatic inspection evaluation and mission planning. In summary, the contribution of this work is an algorithmic approach to simultaneously estimate the marine growth coverage and thickness using common optoacoustic ROV sensors.

II. Materials and Methods

The overall objective of marine fouling load estimation requires knowledge of the 3D distribution of the marine fouling over the structural surfaces. Based on previous work, this will be solved using a two-component approach; estimating the surface coverage distribution, and estimating the coverage thickness, with the estimation conducted at known robot locations in order to construct a complete fouling estimate as a function of depth from the surface.

A. Sensors

The sensing solution consists of two commercial off-the-shelf sensors mounted in a forward-facing orientation on an ROV. The visual sensing is conducted using an off-the-shelf RGB camera with HD resolution mounted in a dome window waterproof enclosure. The acoustic thickness sensing is undertaken using the BluePrint Subsea Oculus m3000d sonar [8] set to $3000\,\mathrm{kHz}$ and $1\,\mathrm{meter}$ sensing range for the highest possible spatial resolution; in this configuration, the sonar best-case resolution is $2\,\mathrm{mm}$ and the field-of-view is 40° horizontal by 20° vertical (half-power).

B. Data acquisition and storage

For both the camera and sonar, the data has been stored in a ROS-bag [9] which logs the raw sonar image using an open-source driver from [10], and the H265 compressed visual feed using the ROS webcam driver from [11]. Additionally, the robot operating depth is extracted from the onboard pose estimation system and saved to allow for correlating the exteroceptive sensor data to the current operating depth for each camera and sonar data frame. Due to the inherent asynchronous sensing, the data must be synchronized, which has been performed using the MATLAB function synchronize [12]. The synchronization is based on the sonar timestamps given that they have the lowest rate; these three measurements are thus combined to form a complete time synchronized table as illustrated in the code listing 1

```
%% Make new timetable with "nearest" to sonar
    times
table_complete = synchronize(timetable_color,
    timetable_sonar, timetable_pose,
    SonarTimeRaw, 'nearest');
```

Listing 1: Synchronization code

C. Marine-fouling coverage estimation

The estimation of marine fouling coverage is performed using a DeepLabV3+ deep-neural segmentation network, applying the network weights developed for marine-growth segmentation developed in [13]. The images from a forward-facing camera pointing directly towards the structure have been input into the neural network, returning the segmentation of the image into hard and soft marine growths, structure, and background classes. Within the segmentation output, the bounding box of the nearest structural member has been manually delimited; then the count of each pixel class against the size of the the bounding box has been evaluated. This thus yields a percentage coverage for the hard and soft marine growth, respectively, as illustrated in the code of listing 2. An example of the input image and resulting coverage calculated coverage percentages is shown on fig. 1 with the segmented color overlay shown in the top part and fouling percentage plot shown below with matching coloration to the overlay. It's visible that the main detected types on the structural surfaces are the seaweed and anemone classes, with some parts of clean structural surfaces detected.

```
image_u16 =
    im2uint16(table_complete.Visual.Image{i,1});
[output_seg, score, all_score] =
    semanticseg(image_u16,foulingsegnet);
AOIseg = output_seg(:,140:500);

[N,X] = histcounts(AOIseg,
    'Normalization','probability');
table_complete.Hard_fouling_coverage(i) =
    sum(N(4:5));
table_complete.Soft_fouling_coverage(i) =
    sum(N(6:7));

```

Listing 2: Coverage code

D. Marine-fouling thickness estimation

For the marine thickness estimate, the HF-sonar ping result images have been evaluated. The image consists of a 2D fan covering the fan 12° by 2 meters facing directly towards the marine-growth-covered surface. The analysis is performed by collapsing the 2D sonar image into a 1D signal by summing over the width of the image, thus in essence combining the echo from the marine growth over the entire imaging width, as shown in the code of listing 3. At the nominal distance of $20\,\mathrm{cm}$ from the surface, the swath width and height is $\approx 15\,\mathrm{cm}$ by $\approx 7\,\mathrm{cm}$.

```
%% Normalize input data
data = sum(table_complete.Sonar.Image_raw{i})/
    (512*256).';
%% Find peaks
[pks,locs,wdths,prom] = findpeaks(data,
    linspace(
    sonardata.SpacialReference.YWorldLimits(1),
    sonardata.SpacialReference.YWorldLimits(2),
    512),'NPeaks',1,'SortStr','descend');
%% Save peak width as thickness
table_complete.Thickness(i) = wdths;

```

Listing 3: Thickness estimate code

The resulting 1D signal relates to the cumulative acoustic reflection of the material in the swath, with respect to the distance from the sonar. Using a simple peak detection algorithm [14], the most prominent peak, corresponding to the marine growth, has been found. The thickness of the marine growth is then found by thresholding around this peak at 50% of peak value. A caveat of this approach is that any object interceding between the sonar and structural member will be evaluated as part of the marine growth (even if transient in nature, such as floating debris).

An example of the output is shown on fig. 2, with the sonar 2D cross-section image given at the top, and the 1D return signal annotated with the peak-detection and thickness (width) estimate illustrated below.

III. Case study - Coastal mooring post

The estimation algorithm has been tested in a coastal test site where a mooring post with heavy marine-growth in a $15\,\mathrm{meter}$ deep harbor on the east coast of Jutland, Denmark. The inspection has been performed using the *COALA* robot, described in [15]; on the robot, the sonar and camera are mounted in close proximity, and with aligned axes.Illustrative individual results of the segmentation results are shown on fig. 1 and thickness measurements are shown in fig. 2.

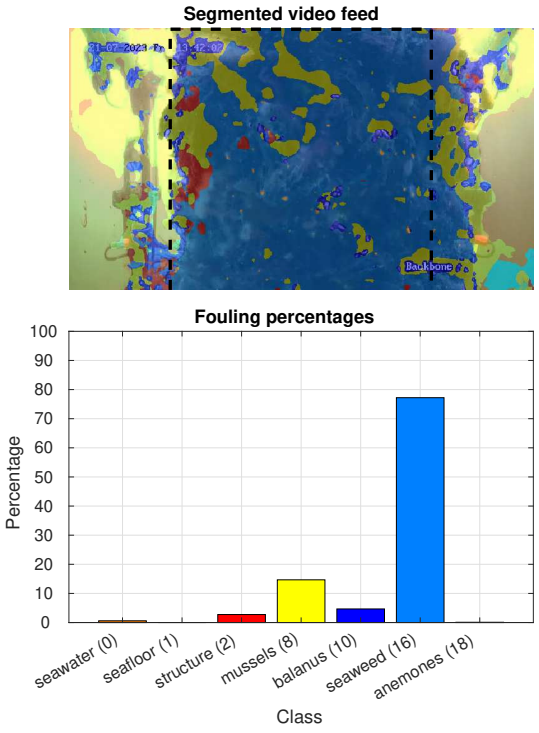

Fig. 1: Example sonar coverage estimation

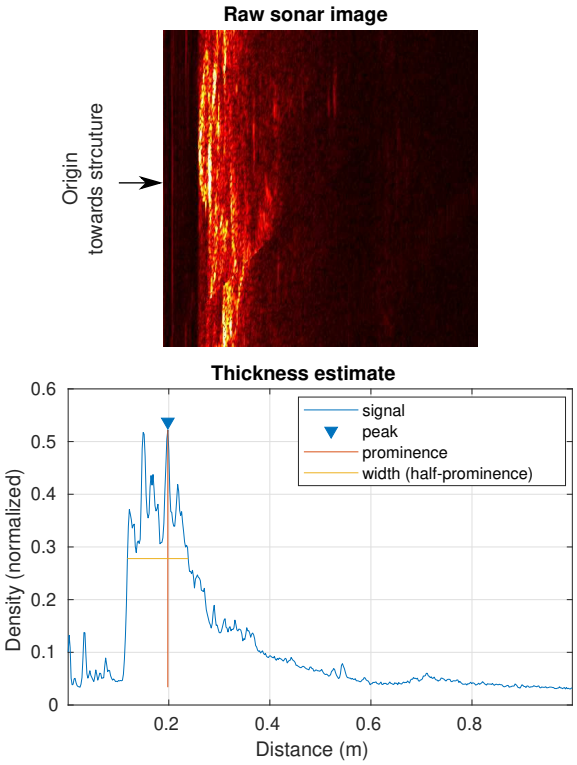

Fig. 2: Example sonar thickness estimation

The plot on fig. 3 shows the combined assessed marine coverage for a mooring post, showing the expected decrease in soft-marine growth with increasing depth (due to decreased photosynthetic activity at depth, in line with [16]).

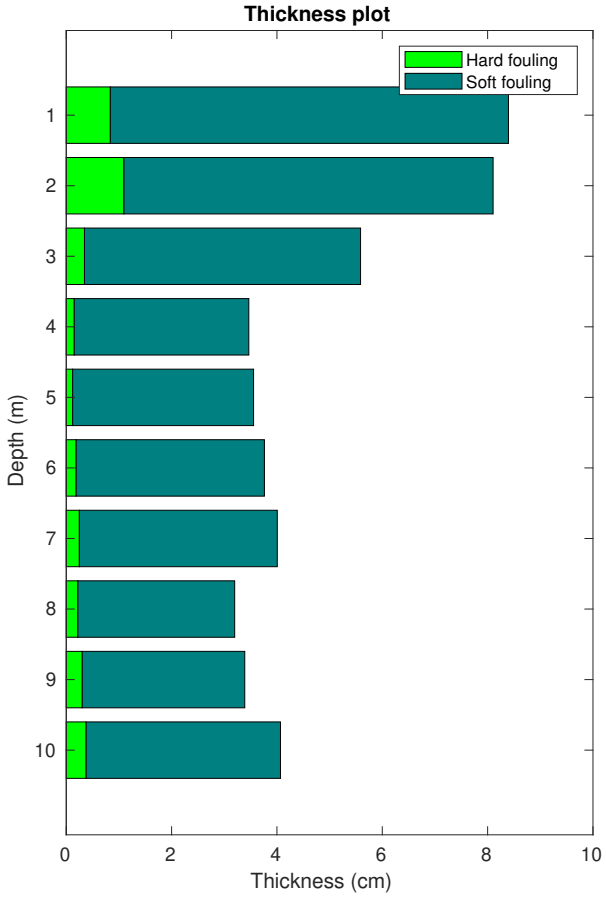

Fig. 3: Example opto-acoustic combined estimate

IV. Conclusion

The presented methodology has a strength in the use of existing sensors on the robot, in particular, the camera and sonar are already present and required by the pilot, for navigation of the robot and manual identification of target objects and features; thus the additional automatic inspection algorithms represent a low-cost, software-only, addition to the existing ROV inspection platform and method. The combined measurement algorithm has yielded promising results which correspond to known species distribution shown in [16], however, there is a need for extensive validation of the accuracy of both the thickness measurement and the validity of the assessed species coverage. This will most likely include the use of an expert reference assessment as a gold standard, which will be explored in future work. For the marine growth thickness evaluation, recording and modeling the

acoustic reflection of various marine species represents an avenue of future work, since data on the specific acoustic impedance of underwater biological materials is rarely readily available, although some works have demonstrated artificial marine growth in controlled environments [17]. Another possibility is to extend the algorithm for marine-growth thickness estimation with species determination or rejection of transient effects, which are currently not included. For the marine growth coverage estimation, the incorporation of additional species and additional test site evaluations remains relevant in future work. To increase overall estimate spatial accuracy, accurate co-registration between the sonar and visual sensing signals, as well as the robot orientation should be implemented such that the estimate can be precisely referenced to the structural surface positions, rather than just depth.

ACKNOWLEDGEMENTS

The authors would like to thank for the support from the Energy Technology Development and Demonstration Program (EUDP) via the "ACOMAR – Auto Compact Marine Growth Remover" project (J.No. 64020-1093). Thanks to partners SubC Partner, Sihm Højtryk, Mati2ilt, EIVA, Total E&P Denmark and Siemens Gamesa Renewable Energy, and our colleagues from Aalborg University, for many valuable discussions and technical support: We thank Inter Terminals EOT A/S and Aabenraa Havn for test-site access.

REFERENCES

[1] S. Pedersen, J. Liniger, F. F. Sørensen, and M. v. Benzon, "On Marine Growth Removal on Offshore Structures," in *Proc. of IEEE OCEANS 2022 Chennai*, 2022, DOI: 10.1109/OCEANSChennai45887.2022.9775498.

[2] J. Liniger, A. L. Jensen, S. Pedersen, H. Sørensen, and C. Mai, "On the Autonomous Inspection and Classification of Marine Growth on Subsea Structures," in *Proc. of the IEEE OCEANS 2022 conference*, Chennai, 2022, pp. 1–6, DOI: 10.1109/OCEANSChennai45887.2022.9775295.

[3] F. Schoefs, "Assessing and Modeling the Thickness and Roughness of Marine Growth for Load Computation on Mooring Lines," in *Floating Offshore Wind Turbines (FOWT) 2019*, 2019, DOI: 10.13140/RG.2.2.30142.33604.

[4] F. Schoefs, M. O'byrne, V. Pakrashi, *et al.*, "Fractal Dimension as an Effective Feature for Characterizing Hard Marine Growth Roughness from Underwater Image Processing in Controlled and Uncontrolled Image Environments," *Journal of Marine Science and Engineering 2021, Vol. 9, Page 1344*, vol. 9, no. 12, p. 1344, Nov. 2021, ISSN: 2077-1312, DOI: 10.3390/JMSE9121344.

[5] B. Gaurier, G. Germain, J.-V. Facq, L. Baudet, M. Birades, and F. Schoefs, "Marine growth effects on the hydrodynamical behaviour of circular structures," *14èmes journées de l'Hydrodynamique*, no. November, 2014, [Online]. Available: http://archimer.ifremer.fr/doc/00247/35821/.

[6] H. Ameryoun, F. Schoefs, L. Barillé, and Y. Thomas, "Stochastic modeling of forces on jacket-type offshore structures colonized by marine growth," *Journal of Marine Science and Engineering*, vol. 7, no. 5, May 2019, ISSN: 20771312, DOI: 10.3390/JMSE7050158.

[7] N. J. Heaf, "The Effect of Marine growth on the performance of fixed offshore platforms in the North Sea," *Proceedings of the Annual Offshore Technology Conference*, vol. 1979-May, pp. 255–267, ISSN: 01603663, DOI: 10.4043/3386-MS.

[8] Blueprint Design Engineering Ltd, *Oculus m-series*, 2022, [Online]. Available: https://www.blueprintsubsea.com/oculus/oculus-m-series.

[9] *rosbag - ROS Wiki*, [Online]. Available: http://wiki.ros.org/rosbag.

[10] UW APL Ocean Engineering, *oculus_sonar_driver*, [Online]. Available: https://gitlab.com/apl-ocean-engineering/oculus_sonar_driver.

[11] *video_stream_opencv - ROS Wiki*, [Online]. Available: http://wiki.ros.org/video_stream_opencv.

[12] The MathWorks Inc., *MATLAB synchronize*, [Online]. Available: https://se.mathworks.com/help/matlab/ref/timetable.synchronize.html.

[13] C. Mai, C. Wiele, J. Liniger, and S. Pedersen, "Synthetic Subsea Imagery for Marine-Growth Inspection under Natural Lighting."

[14] The MathWorks Inc., *MATLAB findpeaks*, [Online]. Available: https://se.mathworks.com/help/signal/ref/findpeaks.html.

[15] S. Klemmensen, R. Olsen, K. Turner, F. F. Sørensen, and M. Von Benzon, "COALA - A Novel Approach to Offshore Tubular Inspection and Cleaning," *OCEANS 2023 - Limerick, OCEANS Limerick 2023*, 2023, DOI: 10.1109/OCEANSLIMERICK52467.2023.10244571.

[16] I. Jusoh and J. Wolfram, "EFFECTS OF MARINE GROWTH AND HYDRODYNAMIC LOADING ON OFFSHORE STRUCTURES," in *Jurnal Mekanikal*, vol. 1, 1996.

[17] R. Baarholm and K. Skaugset, "Modelling and Characterization of Artificial Marine Growth," *Proceedings of the International Conference on Offshore Mechanics and Arctic Engineering - OMAE*, vol. 5, pp. 863–870, Jul. 2009, DOI: 10.1115/OMAE2008-57587.